photonics

MDPI

Article

Power-Scaled Mode-Locked Femtosecond Pulses from an All-Polarization-Maintaining Tm-Doped Figure-9 Fiber Laser

Mingrui Jiang [1], Ting Wen [1], Yuhang Wei [1], Liang Zhao [1], Senyu Wang [1], Jinlong Wan [1], Hongyu Luo [1] and Jianfeng Li [1,2,*]

[1] State Key Laboratory of Electronic Thin Films and Integrated Devices, School of Optoelectronic Science and Engineering, University of Electronic Science and Technology of China (UESTC), Chengdu 610054, China; 202411050816@std.uestc.edu.cn (M.J.)
[2] Tianfu Jiangxi Laboratory, Chengdu 641419, China
* Correspondence: lijianfeng@uestc.edu.cn

Abstract

We demonstrate an all-polarization-maintaining (PM) mode-locked thulium-doped fiber laser operating in the net-normal-dispersion regime based on a figure-9 nonlinear amplifying loop mirror (NALM) configuration. A chirped fiber Bragg grating (CFBG) and a commercial PM dispersion-compensating fiber (PM-DCF) are incorporated into the figure-9 cavity, providing a large normal net dispersion and enabling stable dissipative-soliton mode-locking. Under stable dissipative-soliton operation, the laser delivers a maximum output power of 53.6 mW at a repetition rate of 12.31 MHz, corresponding to a pulse energy of 4.3 nJ. The output spectrum has a central wavelength of ~1952 nm with a 3 dB bandwidth of ~11 nm. The all-PM laser oscillator directly generates a fs pulse without extra-cavity compression, achieving a pulse duration of 545 fs at the CFBG arm. Moreover, stable fundamental mode-locking is verified by a high radio-frequency signal-to-noise ratio (SNR) exceeding 82 dB and a long-term root-mean-square (RMS) power fluctuation of 0.45% over two hours. To the best of our knowledge, this represents the highest output power generated from an all-PM-fiber figure-9 laser oscillator in the 2 μm band, alongside fs-pulse operation. This high-power, compact, stable and environment-insensitive fs-pulsed laser source shows great potential as an ideal seed for biomedical imaging and mid-infrared frequency combs.

Keywords: mid-infrared; fiber laser; ultrafast laser

1. Introduction

Mode-locked (ML) thulium-doped fiber lasers (ML-TDFLs) with high power, high energy, exceptional stability and ultrafast temporal characteristics have attracted significant attention due to their critical applications in biomedical treatment [1,2], precision material processing [3,4], laser lidar systems [5] and frequency combs [6]. Therefore, the development of high-power, ultrashort-pulse ML-TDFLs has remained an active research topic in recent years. Although chirped pulse amplification (CPA) is a common approach to generating high-power, high-energy fs pulses at 2 μm, it suffers from a complex system architecture and an inevitable reliance on free-space optics, which limit its practical applications. In contrast, an ML fiber laser constructed from all-PM-fiber components has the advantages of environmental insensitivity and good robustness, which are crucial for practical applications. Consequently, further research on developing high-power, all-PM, and environmentally stable laser seeds in the 2 μm band is highly desirable.

Check for updates

Received: 29 January 2026
Revised: 25 February 2026
Accepted: 27 February 2026
Published: 2 March 2026

Copyright: © 2026 by the authors. Licensee MDPI, Basel, Switzerland. This article is an open access article distributed under the terms and conditions of the Creative Commons Attribution (CC BY) license.

Similar to fiber lasers operating at the 1 μm and 1.55 μm bands, various methods have been developed to realize high-power, high-energy ultrafast lasers in the 2 μm band. Mode-locking based on real saturable absorbers (SAs) represents a classical approach [7]. Common SA materials for TDFLs include semiconductor saturable absorber mirrors (SESAMs) [8] and low-dimensional materials such as graphene [9], carbon nanotubes (CNTs) [10,11] and black phosphorus (BP) [12]. Using real SAs, several record results have been reported from all-fiber ML-TDFLs, including the highest output power of 84 mW with CNTs [13], the highest single-pulse energy of 4.9 nJ with a SESAM [14], and the shortest pulse duration of 139 fs with BP [12]. However, these SAs suffer from several shortcomings, such as a low damage threshold, limited lifetime under higher saturation fluence, and poor reproducibility in fabrication. Nonlinear polarization rotation (NPR) is another widely used mode-locking mechanism [15,16]. Based on this technique, a high-order soliton laser oscillator was demonstrated [17], achieving a record output power of 90 mW and a pulse duration of 350 fs. In addition, Chernysheva et al. reported a TDF soliton laser based on the co-action of CNTs and NPR [18], which delivered ~500 fs pulses with an average power of 117 mW and a pulse energy of 10.87 nJ. Nevertheless, NPR-based systems are difficult to implement in all-PM-fiber architectures and are vulnerable to environmental disturbances. In contrast, NALM configurations are compatible with all-PM-fiber systems [19,20], offering enhanced environmental stability. Consequently, the robust all-PM NALM technique has become a preferred choice for commercial ultrafast fiber laser systems. Recently, a DCF (PM2000D) was incorporated into an all-PM figure-8 NALM cavity for dispersion management [21]. At a net dispersion of 0.02 ps^2, stable mode-locking operation was achieved with an average output power of 23.8 mW, a single pulse energy of 1.5 pJ, and a pulse duration of 7 ps. The output pulses were further compressed by a grating-pair-based compressor, resulting in the shortest compressed pulse duration of 539 fs.

Notably, the figure-9-NALM has attracted increasing attention owing to its simple structure and high flexibility, leading to numerous practical implementations in recent studies. It has been widely applied in the 1 μm and 1.55 μm bands [22–24], with several commercial products. A variety of high-performance results have been reported, including MLFLs with different net dispersion values [25], fs-level pulses [22,23], high output power [26] and ultrahigh SNR [24]. In the 2 μm band, an all-fiber figure-9 structure was first reported for generating dissipative-soliton resonance (DSR) pulses with ns-level duration in 2019 [27]. This oscillator delivered an average output power of up to 0.67 W at a repetition rate of 318 kHz. It is worth noting, however, that this cavity was not constructed with all-PM-fiber. In 2022, the first all-PM fs-level figure-9 ML-TDFL was demonstrated [28]. This laser operated at a repetition rate of 52.4 MHz and a center wavelength of 1985 nm, producing 650 fs pulses with an output power of 9.3 mW and a pulse energy of 177 pJ under single-pulse operation. Nevertheless, the system was not fully fiber-integrated, as its linear arm incorporated a free-space non-reciprocal phase shifter and a polarizing beam splitter. In 2023, Ren. B. et al. demonstrated an all-PM-fiber figure-9 ML-TDFL operating at 1950 nm with a net dispersion of -0.06 ps^2 [29]. At a repetition rate of 30.6 MHz, the laser delivered an output power of 6.5 mW and a pulse duration of 449 fs, corresponding to a pulse energy of 212 pJ. However, the achievable output power and single-pulse energy were fundamentally constrained by the soliton area theorem [30]. More recently, in 2025, Feng et al. investigated the output characteristics of an all-PM figure-9 mode-locked TDF laser equipped with a spatially nonreciprocal phase shifter under different net cavity dispersions [31]. Finally, this laser operated at a repetition rate of ∼27 MHz and a center wavelength of 1933.4 nm, producing dual pulses with durations of 288 fs at output powers up to 177.4 mW. However, the system was not all-fiberized. To date, no high-power, fs-level

pulsed, all-PM-fiber laser based on a figure-9 cavity has been reported in the 2 μm spectral region. The recent studies are summarized in Table 1.

Table 1. Recent studies of mode-locking lasers in the 2 μm band.

Ref.	Mode-Locking Mechanism	Wavelength	Output Power	Pulse Energy	Pulse Duration	SNR	All-PM	All-Fiber Structure
[14]	SA-SESAM	1915 nm	158 mW	4.9 nJ	579 fs	52 dB	No	Yes
[12]	SA-BP	1859 nm	20.4 mW	0.97 nJ	139 fs	60 dB	No	Yes
[17]	NPR	1890 nm	90 mW	7.8 nJ	350 fs	72 dB	No	Yes
[21]	NALM figure-8	1860 nm	23.8 mW	1.5 nJ	7 ps	70 dB	Yes	Yes
[28]	NALM figure-9	1985 nm	9.3 mW	0.18 nJ	1.28 ps	80 dB	Yes	No
[29]	NALM figure-9	1950 nm	6.5 mW	0.21 nJ	469 fs	95 dB	Yes	Yes
This work	NALM figure-9	1952 nm	53.6 mW	4.3 nJ	545 fs	82 dB	Yes	Yes

In this work, we demonstrate a power-scaled, fs-pulsed, all-PM figure-9 ML-TDFL operating in a net normal dispersion regime for the first time. A homemade CFBG and commercial PM-DCFs (Nufern, Saxonburg, PA, USA, PM2000D) were integrated into the cavity for dispersion management, which enabled the successful realization of dissipative-soliton operation with a large net normal dispersion. Highly stable passive mode-locking was self-started through simply turning on the pump power. The ML-TDFL delivers a maximum average output power of 53.6 mW and a single-pulse energy of 4.3 nJ at a repetition rate of 12.31 MHz, with a pulse duration of 545 fs. To the best of our knowledge, this represents the highest average output power of a figure-9 ML-TDML oscillator in the 2 μm band.

2. Experimental Setup and Methods

The experimental setup of the all-PM figure-9 ML-TDFL was depicted in Figure 1, which was mainly composed of two parts: a nonlinear amplifying loop mirror and a linear arm. In the NALM section, a 1570 nm high-stability DFB-type semiconductor laser (Hanyu Co., Shanghai, China, VLSS-1570-M-3W) source was used as the pump source, with a maximum power of 3 W, and a 3 m-long PM Tm-doped fiber (Nufern, Saxonburg, PA, USA, PM-TSF-9/125) was adopted to provide sufficient optical gain. A PM wavelength division multiplexer (PM-WDM) was utilized to combine the 1570 nm pump light with the intracavity oscillating laser. A 2 × 2 PM tapered fiber coupler with a splitting ratio of 45:55 (45:55 OC) was employed to form a fiber loop that allows for interference between the two counter-propagated laser signals (clockwise and counterclockwise in the loop), thereby generating the effect of an equivalent saturable absorber. In addition, a phase shifter (PS) which provides a linear $-\pi/2$ phase bias was inserted in the loop to significantly shorten the required length of the passive fiber and guarantee the self-starting operation of the mode-locking. Based on the typical figure-9 mode-locked structure, two PM-DCFs with lengths of 1.5 m and 2 m were added in the cavity. The position of the PM-DCF was shown in Figure 1, which was of vital significance because its broadening effect on pulses can avoid the distortion due to nonlinear effects caused by high peak power during power amplification [32]. Therefore, we investigated the optimal placement of the PM-DCFs experimentally. Specifically, the best performance was obtained by positioning one 2.0 m length DCF between the PS and SMF, and the other 1.5 m length one immediately before the CFBG; the positions of the DCFs were consistent with those in the previous literature [33]. Here, the function of this DCF before CFBG was to buffer the sudden dispersion changes in short-length CFBG, thus avoiding its adverse effect on mode-locking stability. Therefore,

the dispersion management scheme we implemented, which combines the CFBG and PM-DCF, facilitated the generation of stable dissipative-soliton ML laser pulses.

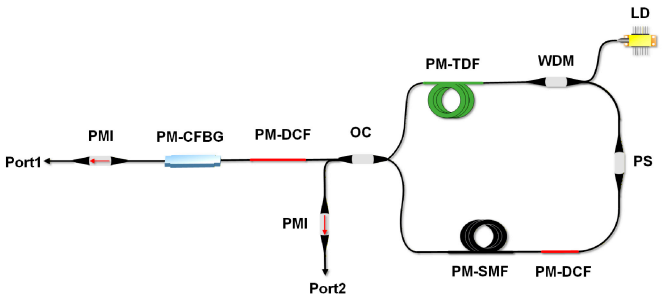


Figure 1. Schematic of an all-fiber, PM thulium-doped fiber dissipative-soliton laser based on a nonlinear amplifying loop mirror (NALM). OC: output coupler; PMI: polarization-maintaining isolator; WDM: wavelength division multiplexer; CFBG: chirped fiber Bragg grating.

For the linear arm section, a homemade PM-CFBG with a center wavelength of 1955 nm and a peak reflectivity of 15% was used; the specific parameters are listed in Table 2. We have developed a novel fabrication method that combines a 257 nm femtosecond laser with a custom-designed chirped phase mask (linear chirped rate: ~13.8 nm cm^{-1}) for writing CFBGs on a H_2-loaded PM fiber [34]. It functioned not only as a cavity mirror but also as a component to introduce normal dispersion, with a dispersion coefficient of approximately 0.98 ps^2. The total length of the resonant cavity was around 17.2 m. The group velocity dispersion (GVD) of the PM single-mode fiber, the PM Tm-doped fiber and the PM2000D used in the cavity were approximately -0.068 ps^2/m, -0.076 ps^2/m and 0.065 ps^2/m, respectively. Based on this, the calculated net cavity dispersion was about 0.25 ps^2. The laser outputs were extracted from port 1 of the CFBG and port 2 of the fiber loop, respectively. Two PM isolators were integrated into each output branch to effectively suppress the influence of end-face reflection on the mode-locking stability. After the isolator, a patch cord was connected to the measurement system for evaluating the performance of the output pulses.

Table 2. Parameters of CFBG.

Parameters	Date	Unit
Center wavelength	1955	nm
Reflection Bandwidth (@3 dB)	20.2	nm
Reflectivity	~15	%
D_2	−0.485	ps/nm
β_2	0.98	ps^2

The measurement equipment used for performance characterization includes an optical spectrum analyzer (Yokogawa, Tokyo, Japan, AQ6375), which was used to measure the output optical spectrum of the laser. The temporal waveform of the pulse was collected by connecting a high-speed photodetector (EOT, Traverse City, MI, USA, ET-5000F) to a digital oscilloscope (RIGOL, Suzhou, China, MSO4054), while the radio frequency (RF) spectrum of the pulse train was measured by an RF spectrum analyzer (Rohde & Schwarz, Munich, Germany, FSV3007). The pulse width was measured using a commercial autocorrelator (APE, Berlin, Germany, Pulsecheck USB 150).

3. Experimental Results and Discussion

The ML operation was first conducted without the dispersion management of PM-DCFs. Employing the setup in Figure 1 with a 10.5 m PM-SMF and no PM-DCF, initial

experiments were conducted to examine the influence of net dispersion on the mode-locking dynamics. In this case, the net cavity dispersion was calculated to be -0.29 ps^2. When the pump power was increased to 1 W, the laser entered the continuous-wave operating state. As the pump power was increased to 1.4 W, a clear soliton splitting phenomenon was observed. Due to the interaction between higher-order dispersion and nonlinear effects, its periodic evolution is disrupted. By reducing the pump power to ~620 mW, single pulse mode-locking was established with an output power of 2.16 mW and 0.35 mW at port 1 and port 2, respectively. Figure 2a presents the spectra from both output ports, measured with a 0.05 nm resolution. At this pump power, the spectrum from port 1 was centered at 1955 nm with a 3 dB bandwidth of 10.55 nm, whereas that from port 2 exhibited a narrower 3 dB bandwidth of 5.16 nm at the same central wavelength. Both output ports exhibited symmetric Kelly sidebands, which result from gain and loss perturbations experienced by the soliton during propagation in the anomalous-dispersion regime [35,36]. The measured pulse train was depicted in Figure 2b, revealing a consistent temporal spacing of 87 ns between pulses. This interval aligned well with the calculated round-trip time of the 18.5 m long cavity, confirming the expected repetition rate. The RF spectrum was measured over a 1 MHz span with a resolution bandwidth (RBW) of 10 Hz, as illustrated in Figure 2c. An SNR of 91 dB was obtained, confirming the excellent stability of the mode-locking operation. Such ultrahigh-SNR performance in a figure-9 cavity at 2 μm was consistent with previous reports [29]. The autocorrelation trace of the uncompressed output pulse from port 1 was shown in Figure 2d, revealing a Gaussian-fitted pulse duration of 1.43 ps (corresponding to a Fourier-transform-limited duration of 0.53 ps), indicating that the output pulse was strongly chirped. The observed ps-level pulse width was attributed to the broadening in the anomalous-dispersion passive fiber following the CFBG and PMI. These low power levels were fundamentally limited by the soliton area theorem, which constrained the pulse energy and average power achievable in conventional soliton ML systems. To overcome this limitation, we introduced PM-DCFs (Nufern, Saxonburg, PA, USA, PM2000D) into the figure-9 cavity, enabling stable single-pulse dissipative-soliton mode-locking in the net normal dispersion regime.

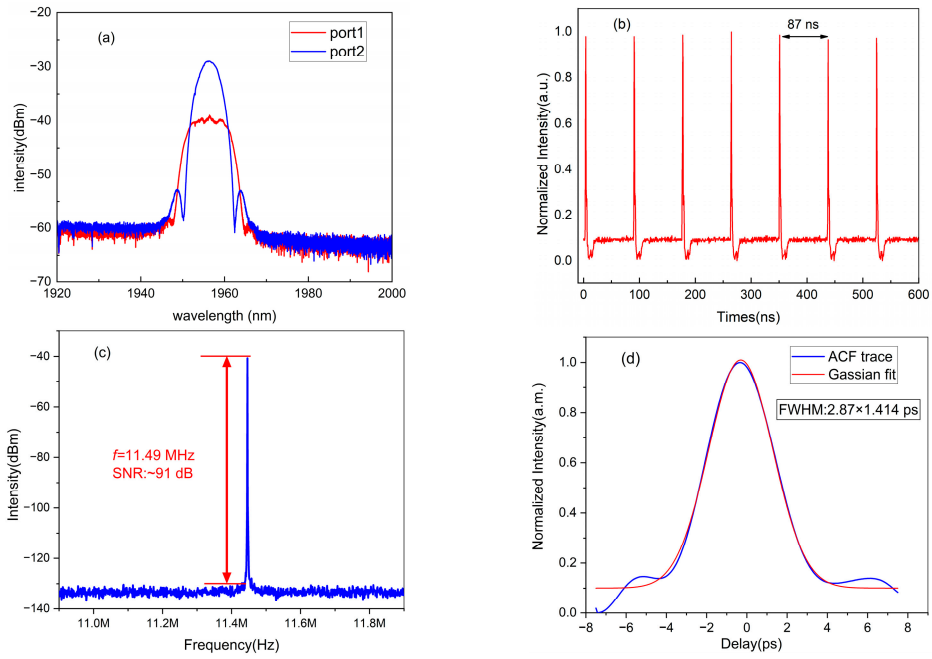


Figure 2. Output characteristics of port 1 without DCF: (**a**) output spectra, (**b**) the pulse train, (**c**) RF spectrum of the output signal and (**d**) autocorrelation trace.

By alternately using positive and negative dispersion optical fibers and taking advantage of their characteristics to reduce the average dispersion of the entire optical fiber transmission link, the interaction between solitons during transmission can be improved. This periodic broadening–compression process effectively reduces the peak power and limits the built-up nonlinear phase shift, thereby preventing wave-breaking [37]. Thus, two commercial PM-DCFs with lengths of 1.5 m and 2 m were inserted into the cavity, as shown in Figure 1. Self-stating mode-locking in a single-pulse state was achieved at the pump power of 1.8 W. Upon initiation, the ML operation could be maintained when the pump power was slightly reduced. The laser reverted to CW mode when the pump power was reduced below 1.45 W. The single-pulse state persisted as the pump power was increased up to 2.9 W. The measured ML spectra with different pump powers of port 2 under single-pulse operation are shown in Figure 3a. At the maximum pump power of 2.9 W, the spectrum exhibited a center wavelength of 1952 nm and a 3 dB bandwidth of 11.2 nm, corresponding to a Fourier-transform-limited (FTL) pulse duration of 500 fs. Figure 3b presents the recorded pulse train from port 1. The measured pulse train exhibited a temporal spacing of 81.2 ns, which matched well with the round-trip time of the 17.2 m long cavity. This confirms that the laser operated at the fundamental repetition rate of 12.31 MHz, with no additional pulses observed. Figure 3c illustrates the RF spectrum with a frequency range of 10 MHz and an RBW of 100 Hz. The SNR reached 82 dB, indicating the excellent stability of the mode-locking operation. The autocorrelation trace of the output pulse from port 1, measured without external compression, is presented in Figure 3d. A Gaussian-fit pulse duration of 545 fs was obtained, corresponding to approximately 1.1 times the FTL. In this dispersion-managed TDFL, the pulse chirp and width vary periodically at different locations within the cavity. Overall, after stable mode-locking is achieved, the laser exhibits excellent stability with nearly linear output power scaling, constant pulse duration, high RF SNR, and no saturation behavior within the investigated pump range.

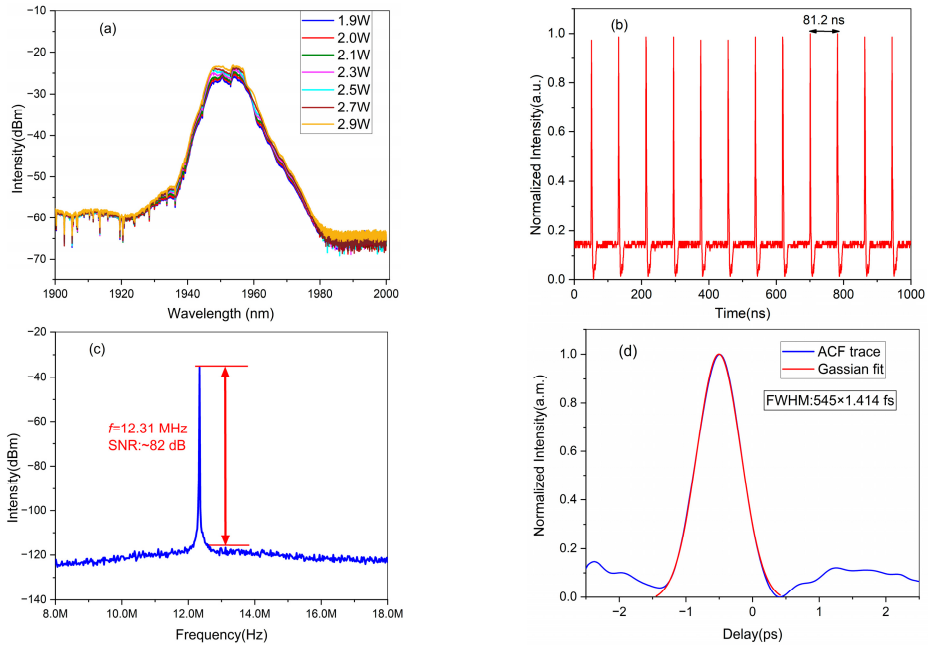


Figure 3. (**a**) Output spectra of port 1 at different powers, (**b**) the pulse train, (**c**) RF spectrum of the output signal and (**d**) autocorrelation trace.

An interesting phenomenon was observed wherein the spectrum was deviated from that of typical dissipative solitons, exhibiting characteristics intermediate between the

dissipative and stretched solitons. This behavior could be attributed to the combined effect of the CFBG and PM-DCFs on intracavity pulse evolution and dispersion management.

The total round-trip dispersion, calculated from the measured dispersion coefficients of each cavity segment, was 0.25 ps^2, confirming operation in a net-normal-dispersion regime. Meanwhile, the local dispersion accumulated in individual sections (e.g., +0.98 ps^2 in the CFBG) was significantly larger than the net dispersion, indicating a strongly dispersion-managed cavity. Such a large dispersion contrast inevitably induced periodic pulse breathing during each round-trip.

For the measured pulse duration of 545 fs, the corresponding dispersion length was approximately 0.42 m, which was much shorter than the total cavity length (17.2 m), indicating substantial dispersive evolution within each round-trip from the calculated peak power of ~15 kW (twice the output peak power) at the compression point. With a typical nonlinear coefficient $\gamma \approx 1.5\ W^{-1}km^{-1}$ at 2 μm, the nonlinear length was approximately 4 cm [38]. This indicated that Kerr nonlinearity plays a significant role in spectral shaping, while strong dispersion management prevents excessive nonlinear phase accumulation.

In addition, with the increase in pump power and pulse energy (up to 4.3 nJ), the spectral bandwidth narrowed and the sharp, steep edges became flattened (consistent with the inverse relationship between pulse energy and spectral shape reported in Ref. [39]), which further modulated the spectral shape and enhanced the intermediate characteristics.

Therefore, the coexistence of net-normal dispersion, strong dispersion management, and substantial but controlled nonlinear interaction naturally leads to spectral characteristics intermediate between classical dissipative solitons and stretched solitons. The above physical mechanism is fully supported by our experimental data (spectral evolution with pump power, intracavity dispersion parameter calculation) and the mature theoretical conclusions on dispersion-managed dissipative-soliton dynamics in 2 μm Tm-doped fiber lasers [40,41], and can well explain the observed spectral characteristics.

In this experiment, the pump power was increased to 1.8 W (mode-locking threshold) to initiate self-starting mode-locking. Then, the pump power was slightly reduced to the range of 1.5–1.6 W, at which point a precise dynamic balance was established among intracavity gain and loss, dispersion and nonlinear effects. The mode-locking state entered a stable phase without mode hopping or soliton splitting. On the basis of stable mode-locking, a single-pulse output of 53.6 mW was achieved at a pump power of 2.9 W, corresponding to a single pulse energy of 4.3 nJ. To the best of our knowledge, this represents the highest average output power reported of a figure-9 ML-TDML oscillator in the 2 μm band. As the pump power increased, the output power of the ML laser was recorded, as shown in Figure 4a. It was observed that the rate of output power increase did not slow down as the pump power was raised. The maximum output power achieved here was primarily limited by the available pump power and the damage thresholds of the optical components, suggesting potential for further improvement.

The ML-TDFL operated at room temperature for over two hours, and the power fluctuation was approximately 0.45% root mean square (RMS) at an output power of ~53 mW, as shown in Figure 4b. Evaluating the power stability is essential for verifying the long-term reliability of the mode-locked operation. The ML spectra at the highest pump power at a net cavity dispersion of 0.25 ps^2 from port 1 and port 2 were presented in Figure 4c,d, respectively. The spectrum from port 1 exhibited a center wavelength located at 1952.5 nm with a 3 dB bandwidth of 10.8 nm, while that from port 2 was centered at 1952 nm with a 3 dB bandwidth of 11 nm. Both spectra exhibit the typical features of dissipative solitons with high single-pulse energy, shaped by dispersion management and nonlinear effects within the cavity. The slightly narrower 3 dB bandwidth observed at port 1 is attributed to the spectral filtering effect of the CFBG.

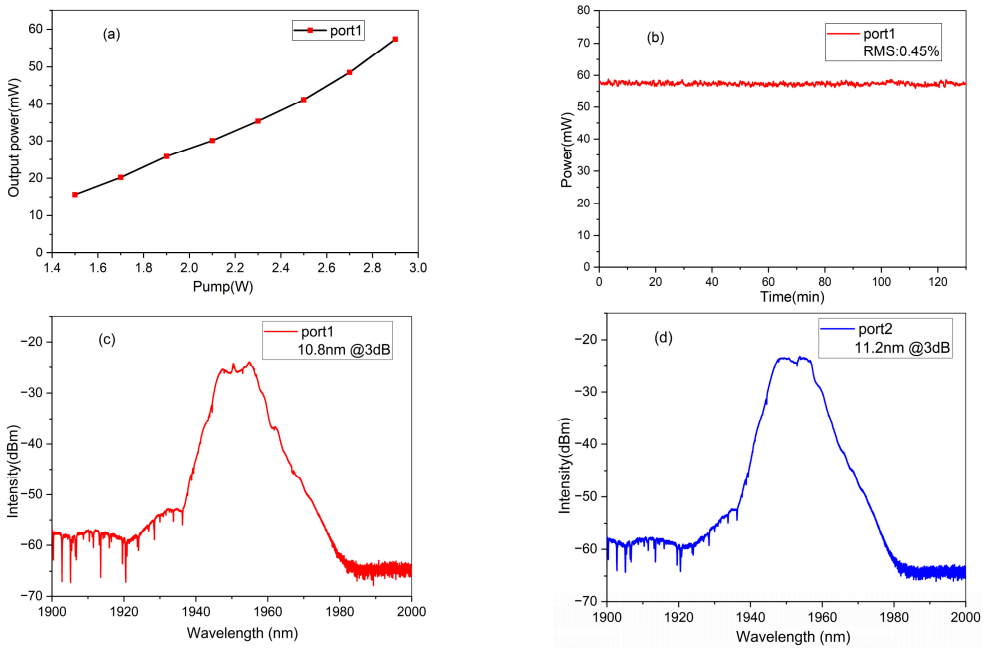


Figure 4. (**a**) Output power of port 1, (**b**) output power evolution with a monitoring time of 2 h, (**c**) output spectra of port 1 and (**d**) port 2.

To further clarify the suppression of excessive nonlinear accumulation, we evaluated the intracavity nonlinear phase shift, defined as $\Phi_{NL} = \gamma \int_0^L P(z)\, dz$ [38], where the local growth rate is proportional to the instantaneous peak power. Although the peak intracavity power at the compression point is estimated to be ~15 kW, the pulse undergoes pronounced dispersion-managed breathing.

Both the PM-DCF and the CFBG contribute to this redistribution of peak power along the cavity [31]. The PM-DCF provides a normal-dispersion segment that stretches the pulse over a continuous propagation length, thereby reducing its peak power before entering the gain and anomalous-dispersion fibers. The CFBG, with its relatively large positive dispersion, further enhances the dispersion-map strength and induces strong temporal stretching prior to pulse compression. As a result, the pulse remains at high peak power only over a limited effective length in the anomalous-dispersion section. Since the nonlinear phase accumulation rate scales as $d\Phi_{NL}/dz = \gamma P(z)$, this temporal broadening directly reduces the accumulated nonlinear phase over most of the cavity.

Considering the estimated nonlinear length at the compression point (~4 cm) and the limited effective compression region, the round-trip nonlinear phase shift is on the order of 10–20 rad (3π–6π), which is consistent with stable dispersion-managed dissipative-soliton operation and well below the wave-breaking threshold. Therefore, the combined action of the PM-DCF and CFBG does not merely tailor the net dispersion but actively redistributes the peak power spatially, suppressing excessive nonlinear phase accumulation while preserving sufficient Kerr nonlinearity for spectral shaping.

4. Conclusions

We have demonstrated an environmentally stable, all-fiber dissipative-soliton ML-TDFL operating at ~1952 nm based on a NALM figure-9 configuration. By incorporating a homemade CFBG and commercial PM-DCFs into the cavity for dispersion management, a net dispersion of ~0.25 ps^2 was achieved, enabling stable single-pulse dissipative-soliton operation. The oscillator delivered a maximum output power of 53.6 mW and a pulse duration of 545 fs at a repetition rate of 12.31 MHz, corresponding to a single-pulse energy of 4.3 nJ. The mode-locking stability was confirmed by an RF SNR of 82 dB. Furthermore, the

laser exhibited excellent long-term stability, with an RMS power fluctuation of only 0.45% over two hours of continuous operation at room temperature. These results demonstrate the great potential of this high-power, environmentally robust, fs-pulsed ML-TDFL as a practical seed source for biomedical multiphoton imaging and mid-infrared frequency combs generation.

Author Contributions: Conceptualization, J.L. and M.J.; methodology, H.L. and M.J.; software, L.Z.; validation, T.W.; formal analysis, Y.W.; investigation, M.J.; resources, J.L., S.W., and J.W.; data curation, M.J.; writing—original draft preparation, M.J. and T.W.; writing—review and editing, J.L. and H.L.; visualization, M.J.; supervision, J.L.; project administration, J.L.; funding acquisition, J.L. All authors have read and agreed to the published version of the manuscript.

Funding: The authors are grateful for the financial support from the National Natural Science Foundation of China (62575051), Equipment Pre-research Joint Fund of the Ministry of Education (8091B042228), Science and Technology Project of Sichuan Province (2023NSFSC1964, 2023NSFSC0033), and Stability Support Special Project of the Southwest Institute of Technical Physics (No. 2024-WZ-9).

Institutional Review Board Statement: Not applicable.

Informed Consent Statement: Not applicable.

Data Availability Statement: The original contributions presented in this study are included in the article. Further inquiries can be directed to the corresponding authors.

Conflicts of Interest: The authors declare no conflicts of interest.

References

1. Tunc, B.; Gulsoy, M. Tm: Fiber laser ablation with real-time temperature monitoring for minimizing collateral thermal damage: Ex vivo dosimetry for ovine brain. *Lasers Surg. Med.* **2013**, *45*, 48–56. [CrossRef]
2. Xu, D.Y.; Bourdakos, K.N.; Crisford, A.; Johnson, P.; Abughazaleh, I.; Srisamran, P.; Oreffo, R.O.C.; Mahajan, S.; Richardson, D.J.; Xu, L. All-fiberized 1840-nm femtosecond thulium fiber laser for label-free nonlinear microscopy. *Biomed. Opt. Express* **2023**, *14*, 4520–4530. [CrossRef]
3. Wang, Z.H.; Zhang, B.; Liu, J.; Song, Y.F.; Zhang, H. Recent developments in mid-infrared fiber lasers: Status and challenges. *Opt. Laser Technol.* **2020**, *132*, 106497. [CrossRef]
4. Wang, X.F.; Liu, J.H.; Jin, Z.G. State switchable Multi-wavelength and Dissipative Soliton Mode locked Tm-doped Fiber Laser Based on a Combination of Nonlinear Amplifying Loop Mirror and Lyot Filter. *Acta Photonica Sin.* **2020**, *49*, 0414001. [CrossRef]
5. De Young, R.J.; Barnes, N.P. Profiling atmospheric water vapor using a fiber laser lidar system. *Appl. Opt.* **2010**, *49*, 562–567. [CrossRef] [PubMed]
6. Zhou, J.Q.; Qi, W.A.; Zeng, X.; Cheng, X.; Jiang, H.W.; Cui, S.Z.; Feng, Y. All-Polarization-Maintaining, Ultra-Compact Tm-Doped Fiber Laser Designed for Mid-Infrared Comb. *IEEE Photonics Technol. Lett.* **2022**, *34*, 89–92. [CrossRef]
7. Gumenyuk, R.; Vartiainen, I.; Tuovinen, H.; Okhotnikov, O.G. Dissipative dispersion-managed soliton 2 μm thulium/holmium fiber laser. *Opt. Lett.* **2011**, *36*, 609–611. [CrossRef]
8. Qian, X.L.; Kong, Y.; Jiao, Y.H.; Wang, Y.F. Mode-locked figure-9 fiber laser assisted by a SESAM for improving signal-to-noise ratio and stability. *Opt. Fiber Technol.* **2024**, *84*, 103785. [CrossRef]
9. Sobon, G.; Sotor, J.; Pasternak, I.; Krajewska, A.; Strupinski, W.; Abramski, K.M. All-polarization maintaining, graphene-based femtosecond Tm-doped all-fiber laser. *Opt. Express* **2015**, *23*, 9339–9346. [CrossRef]
10. Wang, Y.; Alam, S.U.; Obraztsova, E.D.; Pozharov, A.S.; Set, S.Y.; Yamashita, S. Generation of stretched pulses and dissipative solitons at 2 μm from an all-fiber mode-locked laser using carbon nanotube saturable absorbers. *Opt. Lett.* **2016**, *41*, 3864–3867. [CrossRef]
11. Ososkov, Y.; Khegai, A.; Riumkin, K.; Mkrtchyan, A.; Gladush, Y.; Krasnikov, D.; Nasibulin, A.; Yashkov, M.; Guryanov, A.; Melkumov, M. All-PM Fiber Tm-Doped Laser with Two Fiber Lyot Filters Mode-Locked by CNT. *Photonics* **2022**, *9*, 608. [CrossRef]
12. Zhang, Q.; Jin, X.X.; Hu, G.H.; Zhang, M.; Zheng, Z.; Hasan, T. Sub-150 fs dispersion-managed soliton generation from an all-fiber Tm-doped laser with BP-SA. *Opt. Express* **2020**, *28*, 34104–34110. [CrossRef]
13. Pawliszewska, M.; Dużyńska, A.; Zdrojek, M.; Sotor, J. Metallic carbon nanotube-based saturable absorbers for holmium-doped fiber lasers. *Opt. Express* **2019**, *27*, 11361–11369. [CrossRef]

14. Huang, C.Y.; Wang, C.; Shang, W.; Yang, N.; Tang, Y.L.; Xu, J.Q. Developing high energy dissipative soliton fiber lasers at 2 micron. *Sci. Rep.* **2015**, *5*, 13680. [CrossRef]
15. Wang, Q.; Chen, T.; Zhang, B.; Heberle, A.P.; Chen, K.P. All-fiber passively mode-locked thulium-doped fiber ring oscillator operated at solitary and noiselike modes. *Opt. Lett.* **2011**, *36*, 3750–3752. [CrossRef] [PubMed]
16. Ma, W.Z.; Wang, T.S.; Zhang, Y.; Liu, P.; Su, Y.W.; Jia, Q.S.; Bi, M.Z.; Zhang, P.; Jiang, H.L. Widely tunable 2 μm continuous-wave and mode-locked fiber laser. *Appl. Opt.* **2017**, *56*, 3342–3346. [CrossRef]
17. Gao, C.X.; Wang, Z.Q.; Luo, H.; Zhan, L. High Energy All-Fiber Tm-Doped Femtosecond Soliton Laser Mode-Locked by Nonlinear Polarization Rotation. *J. Light. Technol.* **2017**, *35*, 2988–2993. [CrossRef]
18. Chernysheva, M.A.; Krylov, A.A.; Mou, C.; Arif, R.N.; Rozhin, A.G.; Rümmelli, M.H.; Turitsyn, S.K.; Dianov, E.M. Higher-Order Soliton Generation in Hybrid Mode-Locked Thulium-Doped Fiber Ring Laser. *IEEE J. Sel. Top. Quantum Electron.* **2014**, *20*, 1100908. [CrossRef]
19. Hänsel, W.; Hoogland, H.; Giunta, M.; Schmid, S.; Steinmetz, T.; Doubek, R.; Mayer, P.; Dobner, S.; Cleff, C.; Fischer, M.; et al. All polarization-maintaining fiber laser architecture for robust femtosecond pulse generation. *Appl. Phys. B* **2017**, *123*, 41. [CrossRef]
20. Aguer Garay, C.; Hawker, R.; Runge, A.F.J.; Erkintalo, M.; Broderick, N.G.R. 120 fs, 4.2 nJ pulses from an all-normal-dispersion, polarization-maintaining, fiber laser. *Appl. Phys. Lett.* **2013**, *103*, 3550–3554. [CrossRef]
21. Srisamran, P.; Abughazaleh, I.; Gerard, M.D.; Xu, D.Y.; Jung, Y.; Richardson, D.J.; Xu, L. Polarization-maintaining dissipative-soliton mode-locked thulium fiber laser with a nonlinear-amplifying-loop-mirror cavity operating at 1860 nm. *Opt. Express* **2025**, *33*, 16880–16888. [CrossRef]
22. Yuan, S.; Si, L.; Chen, J.N.; Chen, J.Y.; Yu, H. Generation of 99.8 fs, 25 kW Peak-Power, Dispersion-Managed Pulses Directly from an Yb-Doped Figure-of-9 Fiber. *Laser. Mater.* **2022**, *15*, 7038. [CrossRef]
23. Xiong, S.P.; Luo, D.P.; Liu, Y.; Wang, W.C.; Deng, Z.J.; Tang, Z.Q.; Xie, G.H.; Zhou, L.; Zuo, Z.; Gu, C.L.; et al. Investigation of stable pulse mode-locking regimes in a NALM figure-9 Er-doped fiber laser. *Opt. Express* **2023**, *31*, 514–527. [CrossRef]
24. Cheng, H.H.; Zhang, Z.; Pan, R.; Zhang, T.; Feng, Y.; Hu, X.H.; Wang, Y.S.; Wu, S. Compact, repetition rate locked all-PM fiber femtosecond laser system based on low noise figure-9 Er:fiber laser. *Opt. Laser Technol.* **2023**, *158*, 108818. [CrossRef]
25. Shi, Y.H.; Peng, Z.G.; Cheng, Z.C.; Xia, T.; Zhao, H.; Wan, S.Q.; Wang, P. All-Fiber Polarization-Maintaining Dispersion-Managed Figure-of-9 Mode-Locked Laser. *IEEE Photonics Technol. Lett.* **2022**, *34*, 251–254. [CrossRef]
26. Liu, G.Y.; Wang, A.M.; Zhang, Z.G. 84-fs 500-MHz Yb: Fiber-Based Laser Oscillator Mode Locked by Biased NALM. *IEEE Photonics Technol. Lett.* **2017**, *29*, 2055–2058. [CrossRef]
27. Zheng, Z.J.; Ouyang, D.Q.; Ren, X.K.; Wang, J.Z.; Pei, J.H.; Ruan, S.C. 0.33 mJ, 104.3 W dissipative soliton resonance based on a figure-of-9 double-clad Tm-doped oscillator and an all-fiber MOPA system. *Photonics Res.* **2019**, *7*, 513–517. [CrossRef]
28. Łaszczych, Z.; Krakowski, M.; Soboń, G. Mode-Locking Dynamics in an All-PM Figure-Nine Tm-Doped Fiber Laser. *Appl. Sci.* **2022**, *12*, 10613. [CrossRef]
29. Ren, B.; Li, C.; Wang, T.; Guo, K.; Zhou, P. All-Polarization-Maintaining Figure-9 Mode-Locked Tm-Doped Fiber Laser with Amplitude Noise and Timing Jitter Suppression. *J. Light. Technol.* **2023**, *41*, 733–738. [CrossRef]
30. Huang, Q.Q.; Huang, Z.N.; Mou, C.B. Transient soliton dynamics in a mode-locked fiber laser: From stationary to pulsation. *Opt. Lett.* **2021**, *46*, 5683–5686. [CrossRef]
31. Feng, N.; Yuan, Z.R.; Tang, H.T.; Zhou, R.L.; Nakkeeran, K.; Ji, E.C. Dispersion-managed all polarization-maintaining 2 μm mode-locked fiber laser with nonreciprocal phase bias. *Opt. Laser Technol.* **2025**, *183*, 112340. [CrossRef]
32. Ma, W.Z.; Zhao, D.S.; Liu, R.M.; Wang, T.S.; Yuan, Q.; Xiong, H.; Ji, H.Y.; Jiang, H.L. Observation and optimization of 2 μm mode-locked pulses in all-fiber net anomalous dispersion laser cavity. *Opto-Electron. Adv.* **2020**, *3*, 200001. [CrossRef]
33. Pan, Y.J.; Liu, Y.; Ma, T.; Zhu, Y.L. Generation of Sub-50 fs pulses from a 50 MHz Dispersion-Managed Figure-9 Mode-Locked fiber laser. *Opt. Fiber Technol.* **2025**, *93*, 104278. [CrossRef]
34. Wang, S.Y.; Wan, J.L.; Lei, H.; Zhao, L.; Luo, H.Y.; Li, J.F. High reflectivity, ultraflat-spectrum chirped fiber Bragg grating written using low energy UV femtosecond pulses. *Opt. Laser Technol.* **2024**, *176*, 111035. [CrossRef]
35. Gordon, J.P. Dispersive perturbations of solitons of the nonlinear Schrödinger equation. *J. Opt. Soc. Am. B* **1992**, *9*, 91–97. [CrossRef]
36. Dennis, M.L.; Duling, I.N. Experimental study of sideband generation in femtosecond fiber lasers. *IEEE J. Quantum Electron.* **1994**, *30*, 1469–1477. [CrossRef]
37. Tamura, K.; Ippen, E.P.; Haus, H.A.; Nelson, L.E. 77-fs pulse generation from a stretched-pulse mode-locked all-fiber ring laser. *Opt. Lett.* **1993**, *18*, 1080–1082. [CrossRef]
38. Agrawal, G.P. *Nonlinear Fiber Optics*, 5th ed.; Academic Press: Cambridge, MA, USA, 2013.
39. Chong, A.; Wise, F.W.; Renninger, W.H. Properties of normal-dispersion femtosecond fiber lasers. *J. Opt. Soc. Am. B* **2008**, *25*, 140–148. [CrossRef]

40. Wise, F.W.; Chong, A.; Renninger, W.H. High-energy femtosecond fiber lasers based on pulse propagation at normal dispersion. *Laser Photonics Rev.* **2008**, *2*, 58–73. [CrossRef]
41. Kwon, S.Y.; Lee, J.; Lee, J.H. Intracavity pulse formation dynamics of dissipative soliton fiber lasers depending on saturable absorber parameters at 1.9 μm. *Opt. Laser Technol.* **2025**, *181*, 111594. [CrossRef]

Disclaimer/Publisher's Note: The statements, opinions and data contained in all publications are solely those of the individual author(s) and contributor(s) and not of MDPI and/or the editor(s). MDPI and/or the editor(s) disclaim responsibility for any injury to people or property resulting from any ideas, methods, instructions or products referred to in the content.